Measurement of vascular water transport in human subjects using time-resolved pulsed arterial spin labelling.

Bibic, Adnan; Knutsson, Linda; Schmidt, Anders; Henningsson, Erik; Månsson, Sven; Abul-Kasim, Kasim; Åkeson, Jonas; Gunther, Matthias; Ståhlberg, Freddy; Wirestam, Ronnie

Published in:
NMR in Biomedicine

DOI:
10.1002/nbm.3344

2015

Measurement of vascular water transport in human subjects using time-resolved pulsed arterial spin labelling

Adnan Bibic[1*], Linda Knutsson[1], Anders Schmidt[2,3], Erik Henningsson[4], Sven Månsson[5], Kasim Abul-Kasim[6], Jonas Åkeson[3], Matthias Gunther[7], Freddy Ståhlberg[1,8,9], Ronnie Wirestam[1]

Words: 4447

Short title: Measurement of vascular water transport in human subjects using time-resolved PASL

Key words: arterial spin labelling, capillary transfer time, Langevin modelling, microvasculature, blood brain barrier.

[1] Department of Medical Radiation Physics, Lund University, Lund, Sweden
[2] Department of Anaesthesiology and Intensive Care Medicine, Helsingborg Hospital, Helsingborg, Sweden
[3] Department of Anaesthesiology and Intensive Care Medicine, Lund University, Skåne University Hospital, Sweden
[4] Centre for Mathematical Sciences, Lund University, Lund, Sweden
[5] Department of Medical Radiation Physics, Lund University, Skåne University Hospital, Malmö, Sweden
[6] Department of Radiology, Lund University, Skåne University Hospital, Malmö, Sweden
[7] Frauenhofer MEVIS, Bremen, Germany
[8] Lund University Bioimaging Center, Lund University, Lund, Sweden
[9] Department of Diagnostic Radiology, Lund University, Lund, Sweden
* Corresponding author:
Adnan Bibic, Department of Medical Radiation Physics, Lund University Hospital, SE-221 85, Lund, Sweden. E-mail: Adnan.Bibic@med.lu.se

Abbreviations

3D-GRASE – 3D gradient and spin echo

AAL – automated anatomical labelling

ASL – arterial spin labelling

ATT – arterial transit time

BAT – bolus arrival time

BBB – blood-brain barrier

BL – bolus length

CBF – cerebral blood flow

CTT – capillary transfer time

IC – insular cortex

OC – occipital lobe

PS – permeability-surface area product

ROI – region of interest

TTT – total transit time

Abstract – Most approaches to arterial spin labelling (ASL) data analysis aim at providing a quantitative measure of the cerebral blood flow (CBF). The present study, however, focused on measurement of the transfer time of blood water through the capillaries to the parenchyma (referred to as the capillary transfer time, CTT) as an alternative parameter to characterize the hemodynamics of the system. The method employed in the present study is based on a non-compartmental model, and no measurements need to be added to a common time-resolved ASL experiment. Brownian motion of labelled spins in a potential was described by a one-dimensional general Langevin equation as the starting point, and as a Fokker-Planck differential equation for the averaged distribution of labelled spins at the end point, which takes into account the effects of flow and dispersion of labelled water by the pseudorandom nature of the microvasculature and of transcapillary permeability. Multi-TI ASL data were acquired in fourteen healthy subjects on two occasions in a test-retest design, using a pulsed ASL sequence and 3D-GRASE readout. Based on an error analysis to predict the size of a region of interest (ROI) required for obtaining reasonably precise parameter estimates, data were analysed in two relatively large ROIs, i.e., the occipital lobe (OC) and the insular cortex (IC). The average values of CTT, in OC, were 260±60 ms in the first experiment and 270±60 ms in the second experiment. The corresponding IC values were 460±130 ms and 420±139 ms, respectively. Information related to the water transfer time may be important for diagnostics and follow-up of cerebral conditions or diseases characterized by a disrupted blood-brain barrier or disturbed capillary blood flow.

Introduction

Arterial spin labelling (ASL) is a magnetic resonance imaging (MRI) method for measurement of tissue perfusion, employing magnetically labelled endogenous arterial water as a tracer. Determination of tissue perfusion is valuable for characterization of vascular disorders and also for assessment of various physiological and pathophysiological conditions, including acute cerebral ischemia (1), schizophrenia and other psychoses (2,3), as well as various neurodegenerative conditions (4).

ASL is commonly used to measure the cerebral blood flow (CBF), but other microvascular parameters may also be assessed using ASL data. Recently, the average time required for labelled blood water to pass through the capillary wall, here referred as the "transfer time", was assessed using a two-compartment model (5,6). In this approach, the ASL signal was hypothesized to originate from one intravascular and one extravascular compartment, which could be separated due to significant differences in T2 relaxation times (7,8). By using a multi-TI and multi-TE ASL sequence, the "transfer time" was estimated in cerebral grey matter, on a region-of-interest (ROI) basis. Another investigation of interest in this context concerns assessment of the transfer of water across the blood-brain barrier (BBB), using a combination of ASL and diffusion encoding (9).

Furthermore, Kelly et al. (10) investigated ASL-based transit times in an animal study using a 7T small-bore animal MR system and a continuous ASL pulse sequence. They extracted (i) the time for labelled blood to flow from the labelling region to the vascular compartment of the imaging slice (i.e., the arterial or vascular transit time, ATT (11)), (ii) the time for blood water to move from the

labelling plane to the tissue of the imaging plane, and (iii) the time for intravascular water to distribute through the capillary bed into the parenchyma. The latter transfer time is the most relevant parameter in this context because it might be linked to the physiological characteristics of the microvasculature. The model describes a transport mechanism of labelled water in an explicitly stochastic way, as a combination of advection due to the bulk flow that transports the labelled spins downstream in the large vessels, and, when labelled water is added to the microvascular compartment, as a dispersion process outwards from its source in a diffusive manner. In such an approach, only data from an ordinary time-resolved ASL experiment are needed.

In the present study, we adapted the concept by Kelly et al. (10) to clinical settings in human volunteers, employing a clinical 3 T MRI scanner and a pulsed ASL sequence with 3D-GRASE readout (12), which is likely to be clinically more appropriate because of the lower SAR deposit to the patients. To the best of our knowledge, the model has not previously been applied to a clinical environment.

Methods

Theoretical background

The model used in the present study is a non-compartmental approach, where the Brownian motion of particles (in this case labeled spins) is described by a one-dimensional general Langevin equation as the starting point, i.e., a random motion in a potential (applied by an external force, in this case the bulk flow caused by the pressure gradient from the large vessels to the parenchyma), and

as a Fokker-Planck differential equation for the averaged distribution of labelled spins at the end point.

The label and control images were subtracted to produce ASL-weighted images and these difference maps were denoised by a wavelet-domain filtering method (13), using an in-house-developed computer program implemented in IDL (Interactive Data Language, IDL 7.1, ITT Visual Information Solutions, Boulder, CO, USA). ASL-weighted signal data were extracted from two manually selected intracerebral regions in the denoised difference maps, i.e., the occipital lobe (OC) and the insular cortex (IC). The automated anatomical labelling (AAL) map template (MRIcro, www.mricro.com, version 1.4) was employed to estimate the locations of the ROIs. Figure 1 shows the ROIs overlaid on the ASL-weighted maps and the corresponding AAL maps. The model, given in Eq. 1 and further described in the Appendix, was fitted to the experimental data points obtained from the mean ROI signal.

$$c(V,t) = \frac{C_0}{2} \cdot e^{-\frac{t}{T_1}} \left(\mathrm{erf}\left(\frac{TTT+BL-t}{\sqrt{4 \cdot CTT \cdot t}} \right) - \mathrm{erf}\left(\frac{TTT-t}{\sqrt{4 \cdot CTT \cdot t}} \right) \right) \qquad [1]$$

where T_1 is the longitudinal relaxation time of the tissue, measured by a 3D Look-Locker T_1 quantification technique (14) in the corresponding geometric volume, V is any volume into which labelled spins can flow, at a given time point t (10). BL is the bolus length, which was obtained by fitting a reformulated Buxton model (15) to the denoised experimental data points (according to Eq. 2). A separate estimation of BL was shown to return a better goodness of fit than estimating BL as an additional free parameter in Eq. 1 (data not shown).

Furthermore, *TTT* is the total transit time, i.e., the time for blood plasma to travel from the front edge of the labelling plane to the brain tissue (referred to as *MTT* in (10)), *CTT* is the capillary transfer time, i.e., the time for intravascular water to distribute through the capillary bed into the parenchyma (referred to as the capillary transit time in (10)), and *erf* is the error function (16). The ATT is given by ATT=TTT-CTT. In the model, $c(V,t)$ is the concentration of labelled spins, given by the magnetization difference $\Delta M(t)=M_c(t)-M_l(t)$, C_0 is the initial concentration of inverted magnetization at the labelling plane, and $M_c(t)$ and $M_l(t)$ are the longitudinal magnetizations of a voxel in the imaging plane, for the control and labelled images, respectively.

As mentioned above, *BL* was obtained by fitting a reformulated Buxton model (15) to the denoised experimental data points (Eq. 2):

$$\Delta M(t) = \begin{cases} 0 & 0 < t < BAT \\ \frac{2M_{0B}\cdot CBF\cdot\alpha}{\delta R} e^{-\frac{(BAT)}{T_{1b}}} \cdot \left(1 - e^{-\delta R(t-BAT)}\right) \cdot e^{\frac{-(t-BAT)}{T_{1app}}} & BAT < t < BAT + BL \\ \frac{2M_{0B}\cdot CBF\cdot\alpha}{\delta R} e^{-\frac{(BAT)}{T_{1b}}} \cdot \left(1 - e^{-\delta R\cdot BL}\right) \cdot e^{\frac{-(t-BAT)}{T_{1app}}} & BAT + BL < t \end{cases} \quad [2]$$

where *BAT* is the bolus arrival time (sometimes referred to as the transit delay), M_{0B} is the equilibrium magnetization of arterial blood, α is the achieved degree of inversion (assumed to be 1), *CBF* is the cerebral blood flow (in ml/min/100g), T_{1b} is the relaxation time of blood (T_{1b}=1.66 s at 3.0 T (17) and $\delta R = R_{1b} - R_{1app}$, where R_{1app} is the apparent relaxation rate measured under the inflow of fresh blood magnetization. The fitting parameters were *BAT*, *BL*, T_{1app} and *CBF*.

The underlying fitting processes, with regard to the model in Eq. 1, were accomplished by the curve-fitting routine in Mathematica (Wolfram Research Inc., Version 9.0, Champaign, IL, USA), while fitting of the model in Eq. 2 was accomplished by a modified version of the ROOT/MINUIT class. MINUIT is a physics analysis tool for function minimization, intended to fit a mathematical model or a given user function to measured data (18). The MINUIT package used in this study was a straightforward conversion by R. Brun (http://root.cern.ch/root/html/TMinuit.html) from the original Fortran version to a stand-alone C++ MINUIT package.

Influence of noise, bolus length and systemT1 value on the modelling

To evaluate how noise influenced the model fitting, a synthetic time series was created using Eq. 1, and, in order to match the experimental data, the simulated ASL signal curves were sampled at TIs from 300 to 3000 ms at intervals of 300 ms. The TTT ranged from 1400 to 1800 ms and CTT from 200 to 800 ms, both in intervals of 200 ms, and T1 was set to 1.66 s. This CTT range was selected to correspond to the expected physiological range in humans, based on the measured BAT, the expected transfer time through the BBB (19) and the knowledge that capillary fluid mainly exchanges at the arterial end of the capillary system (20) implying that the capillary transfer time should be shorter than the blood mean transit time (MTT). Furthermore, different amounts of random Gaussian noise (21) were added to the synthetic ASL-weighted data to analyze how different SNR levels affected the model fitting, and to establish the optimal ROI size for data evaluation in vivo. Noise was added from SNR levels of 5 (corresponding to the single-voxel SNR of the ASL experiment) to 100

(corresponding to the expected SNR of a 400-pixel ROI) The SNR was defined as the ratio of the maximal ASL signal in the dynamic time series to the noise standard deviation. For one SNR level (SNR=60), simulations with various fixed BLs (ranging from 800 to 1600 ms) were also carried out. All simulation procedures were repeated 1000 times at each noise level. To estimate the reliability of the calculated value, we used the 95% confidence interval (CI[95%]):

$$CI[95\%] = \pm\frac{1.96\times SD}{x_{true}}\times 100 \qquad [3]$$

where *SD* and x_{true} are the standard deviations and true values, respectively, of the estimates of either CTT or TTT, obtained from simulated data.

Finally, noise-free simulations were carried out to show how CTT, TTT and BL estimates changed when the true T1 value differs from the assumed value, i.e., when the simulated label relaxes with T1 of blood (1660 ms) all the time, in the whole system, whilst we assume, in the model fitting, that it relaxes with T1 of tissue (1450 ms) all the time, in the whole system. These simulations were performed with TTT=1500 ms, CTT=[250, 450] ms and BL=[900, 1100] ms.

Subjects and experimental data collection

Fourteen non-smoking healthy adult volunteers (nine males and five females, age 32±9 years, weight 74±11 kg) were included. Each volunteer was scanned twice to test the repeatability of the proposed method, and the time span between the experiments ranged from six days to seven weeks (24 ± 18 days). The study was approved by the Regional Ethical Review Board in Lund, and written

informed consent was obtained from each volunteer prior to the investigation, after individual oral and written information on the study design and aims.

The dynamic ASL data were acquired using a 3T MRI unit (Magnetom Trio, Siemens AG, Erlangen, Germany), using a labelling scheme based on FAIR (22) in combination with a 3D GRASE signal readout approach (12). The inversions were accomplished by adiabatic hyperbolic secant RF pulses, and the inversion slab width was 140 mm in the slice-selective acquisition, corresponding to the size of the field of view (FOV) in the 3D-encoding direction with an addition of 5 mm on each side. During the non-selective acquisition, as no gradients were used, all spins were inverted by an adiabatic hyperbolic secant RF pulse. The imaging parameters were as follows: FOV 230×202 mm^2, matrix=64×56 (increased to 128×112 by zero filling), 26 projections with a reconstructed slice thickness of 5 mm, TR = 3700 ms, TE = 20.6 ms. The readout oversampling was 23.1% with a bandwidth of 2520 Hz/pixel, and 6/8 partial Fourier in the phase-encoding direction. The readout, phase-encoding and 3D-encoding directions were anterior-posterior, right-left and head-feet, respectively.

Ten time points were acquired, starting at an inversion time (TI) of 300 ms followed by a 300 ms increment between time points. To improve the image quality, the 3D acquisition volumes were divided into two segments and five repetitions of data acquisition were made, with a total acquisition time of 740 s. All images were acquired using a quadrature body coil for transmission and a 12-element phased-array head coil as the receiver coil.

Statistics

Statistical analysis was performed using MedCalc for Windows (v. 12.4.0.0 – 64-bit, MedCalc Software, Mariakerke, Belgium). A two-tailed paired Student's t-test was used to compare mean ATT, CTT and BAT values between the two ROIs measured at two different locations in the brain. In this analysis, the results from the two different experiments in each subject were averaged.

Results

Influence of noise, bolus length and system T1 value on the modelling

The synthetic data provided quantitative measures of the accuracy and precision with which TTT and CTT can be estimated at different levels of SNR. Figure 2 shows box-and-whiskers diagrams (median, 1st and 3rd quartiles within boxes, whiskers with minimum values and values up to 1.5 times the interquartile range, and outliers represented by dots for CTT and TTT at different SNRs (along the x-axis), for input values of TTT=1600 ms, BL=1200 ms and CTT=400 ms.

Corresponding CTT and TTT box-and-whiskers diagrams, for other input values (TTT=1600 ms, BL=[800, 1200, 1600] ms and CTT=[200, 400] ms), at different SNRs, are shown in Figures S1-S2 in the supplementary material. Note the use of different y-axis scales for the different SNR levels for clarity. Probability plots for simulated distributions of TTT and CTT (input values TTT=1600 ms, CTT=200 ms, BL=1200 ms) are given in Figure S3 in the supplementary material.

For SNR=60, Figure 3 and Figure S4 (in the supplementary material) show how the 95% confidence intervals (CI[95%]) of estimated CTTs depended on BL, for different true values of CTT and for TTT=1600 (Fig. 3), TTT=1400 ms (Fig. S4a)

and TTT=1800 ms (Fig. S4b). No marked systematic dependence of the absolute CTT value on BL was seen (data not shown), although the spread in CTT estimates tended to be somewhat larger for the longest BLs investigated. Figure 4 shows the 95% confidence intervals (CI[95%]) of the CTT and TTT values for different SNR levels. These results imply that for SNR=85 (as expected in OC, containing approx. 300 pixels), the 95% CI was ±8.8% around the true CTT value and ±1.4% around the true TTT, while for SNR=60 (as expected in IC, containing approx. 140 pixels) the 95% CIs were 12.1% and 1.9% for TTT and CTT, respectively.

The simulations to analyze worst-case effects of a discrepancy between true and assumed system T1 resulted in deviations from the input values of 8.1-16% for CTT, 4.5-8.4% for TTT and 5.3-9.1% for BL.

Experimental data

The mean T1 in IC was (1570 ± 170) ms (mean ± SD) on the first occasion and (1550 ± 180) ms on the second occasion. In OC, the mean T1 was (1360 ± 100) ms on the first occasion and (1360 ± 130) ms on the second occasion.

Examples of ASL difference maps for varying TIs, before and after the denoising procedure, are provided in Figure S5 in the supplementary material. The extracted OC and IC signal intensity time courses, c(V,t), during the bolus inflow, are shown in Figure 5 for all volunteers and for both ASL sessions (test-retest).

Mean values of ATT, TTT and CTT (with corresponding SDs) for both ROIs are reported in Table 1. Values of CTT and ATT differed significantly between the

two ROIs ($p<0.0001$). Longer ATT values were observed in OC, while CTTs were longer in IC.

Average values of BAT and BL in OC and IC, for both experiments, calculated using Eq. 2, are given in Table 2. The BAT values differed significantly between different ROIs ($p<0.0001$), with longer BAT values observed in OC.

Bland-Altman plots for assessment of the repeatability of CTT values obtained from the two ASL sessions are shown in Figures 6a and 6b. The mean differences between the test and the retest sessions were 9% and 4% in IC and OC ROIs, respectively.

Discussion

The aim of this work was to adapt a preclinically tested quantitative ASL method (10) to a clinical environment, assuming that the extracted parameters reflect the transport of water in the microcirculation. The original implementation of the model was applied to a small-bore MRI scanner in an animal model and employed a continuous ASL (CASL) technique. CASL is less appropriate for clinical applications because of high SAR levels, and a pulsed ASL technique was therefore introduced in this study. The main reasons for using 3D GRASE readout instead of, for example, EPI were (i) to speed up the acquisition, (ii) to reduce SAR due to fewer RF excitation/inversion pulses needed to cover the entire volume and (iii) to increase the SNR (which was the most important factor in this study due to the noise sensitivity of the model). Additionally, the use of QUIPSS II (23) or Q2TIPS (24) approaches to control the width of the bolus may improve quantification. In the present study, however, the choice of Q2TIPS saturation

cut-off time was suboptimal, and an alternative method for bolus length assessment was therefore employed. The present study shows that this model, combined with a clinically available pulsed ASL technique, is also applicable to human volunteers with reasonable results. In addition, simulations of how thermal random noise affects the modeled parameters were used as guidelines for appropriate ROI size selection in the experimental images.

In the paper by Kelly et al. (10), CTT was interpreted as dispersion of intravascular water due to exchange of water from the vasculature to the parenchyma as well as pseudo-diffusion within the microvasculature, and this could relate to the capillary function. Although water is considered to be a diffusible tracer, it is not freely diffusible in the presence of an intact BBB (25,26), so altered CTT may potentially reflect changes in the integrity of the BBB.

It is important to note that the transit times were estimated in the entire volume in which labelled spins can flow, with an average flow and diffusion across the whole system (i.e., from the labeling plane where the bolus is created to the ROI from which signal data are collected). Therefore, values of the transit and transfer times, reported here, describe in statistical terms the average times required for the labelled blood water to pass through the system, from the labelling slab to the extravascular space: CTT is determined by the random pseudo-diffusion nature of motion in the capillaries, in combination with the exchange of labelled spins between capillaries and extravascular water, ATT is determined by the bulk flow and TTT is the sum of CTT and ATT, as defined in the original paper (10). In addition, the reported times are likely to depend on

factors not included in the model, for example, cardiac pulsation and arterial dispersion (27-29). Cardiac pulsations impair the precision of the measurements and act like physiological noise. Arterial dispersion might affect the accuracy of measured transit times and introduce a bias, especially to CTT, because dispersion effects lead to a larger spread in tracer arrival times which, in turn, could be interpreted as prolonged CTT by the present model.

Since neither the individual variability of parameters nor the potential pathophysiological effects were known in advance, it was difficult to estimate the required accuracy. Therefore, we performed simulations before the analysis of experimental data, to predict effects of noise on the model parameters and also to estimate SNR-related measurement accuracy. When relating our simulation results (using a fixed BL of 1200 ms, TTT=1600 ms and CTT=200 ms) to larger (OC) and smaller (IC) experimental ROIs, the simulations indicated that the higher SNR levels (approximately 85) in the analysis of larger ROIs (above 300 pixels) would provide more accurate values of CTT (CI[95%] of ±8.8%), whereas less accurate values of CTT (CI[95%] of ±12.1%) can be expected from the lower SNR levels (approximately 60) corresponding to the analysis of smaller ROIs. It should be emphasized that CTT values obtained with the technique reported here (260-460 ms depending on location) reflect not only exchange of water across the capillary walls but also the geometric properties of the microvasculature in terms of pseudo-diffusion in the microvascular network. Simulations (at SNR=60) predicted that prolonged BL leads to poorer precision, especially at longer CTT (Fig. 3) although no systematic errors in mean CTT were revealed when BL was altered (data not shown).

The model employed in the present study should, primarily, be regarded as a new and independent source of information for interpreting time-resolved ASL data. It is, nevertheless, of some interest to make a general comparison of our CTT values with previously published measures of transfer time obtained with other techniques, as summarized in (19). The parameters obtained in the previous studies can be recalculated in order to be compared with CTT: Capillary permeability-surface area product (PS) values of 104-169 ml/100g/min in the human brain have been reported (30-32), and these values of PS can be inserted in Eq. 4 (5):

$$r_{bl\rightarrow ex}(t) = \exp\left(-\frac{PS}{V_c}\cdot t\right) \qquad [4]$$

where $r_{bl\rightarrow ex}$ is the phenomenological exchange term and V_c is the partial capillary volume fraction, i.e., the fraction of the total blood volume in which exchange occurs (approximately one-third of the volume of the microvasculature).

By assuming V_c to be 1.5 ml/100g (5), the average time for labelled blood water to diffuse across the capillary wall ($T_{bl\rightarrow ex}$) can be estimated to be 533-865 ms. Furthermore, Wang et al. (9) found $\frac{PS}{V_c}$ to be 193±50 min^{-1} corresponding to a $T_{bl\rightarrow ex}$ value of 310±80 ms, while Gregori et al. (5) reported a $T_{bl\rightarrow ex}$ value in OC of 545±54 ms.

OC is supplied by the posterior cerebral artery, and the longer ATT and BAT values in OC were thus expected (29,33). Arterial tracer delay times have previously been reported to be 1000-1300 ms for OC, compared with 500-800

ms for the parietal lobe, a region which, as the IC, is supplied by the middle cerebral artery (33). Hence, the tracer is likely to experience a longer arterial pathway for OC than for IC, before arriving at the tissue, leading to an associated spread in tracer arrival times (29), and this would, if arterial dispersion effects were to be detrimental to the present model, lead to a larger CTT bias for OC. However, our data show *shorter* CTT for OC than for IC, and this seems to imply that dispersion is not a dominating contribution to the CTT estimate in our implementation. Furthermore, previous PET studies in normal volunteers have shown that CBV is higher and MTT(=CBV/CBF) is distinctively longer in OC than in IC (34), and that the arterial blood volume fraction (V_a/CBV) is very low in OC compared with other investigated cortical regions (35). These observations clearly indicate that dissimilarities between the microvascular properties of OC and IC are likely to exist, and this makes the present finding of different CTTs between OC and IC physiologically plausible, for example, due to differences in contributions from microvascular pseudo-diffusion, although the exact mechanisms are difficult to elucidate.

Finally, a test-retest analysis was included to check the repeatability of the method. As shown by the Bland-Altman plot in Figure 6, there is no obvious systematic bias (the mean difference is less than 9%), and no systematic variation over the range of measured absolute values. Despite this, the limits of agreement indicate considerable random variation, as also predicted from our simulations, with less precision in smaller than in larger ROIs.

Relevant assumptions of the model include that the concentration of excited spins is influenced by three mechanisms only, i.e., longitudinal relaxation T1,

transport and diffusion. Transport, in this context, is defined as the bulk motion of the fluid, mainly in the large vessels. Diffusion is defined as the sum of the pseudo-diffusion in the microvasculature and the filtration through the capillary wall. Limitations of the model and analyses include (i) sensitivity to noise, bolus length and system T1 (as investigated by simulations in the present study), (ii) inaccurate head positioning (making it more difficult to select identical intracerebral ROIs on different occasions), (iii) dispersion of tracer not taken into account in the model (primarily arterial dispersion), (iv) arterial throughflow (i.e., labelled through-flowing spins on their way to perfuse downstream voxels), and (v) venous outflow, (i.e., exit of labelled water into the venous system with no exchange over the capillary wall). Sensitivity to arterial dispersion of the tracer can be a serious weakness of the Fokker-Planck model, and any potential influence from arterial dispersion on obtained CTT values should be carefully analyzed, as exemplified by our discussion about expected tracer delays in OC and IC above. Effect of venous outflow may violate the assumption that concentration is a conserved quantity in the model. However, this effect should normally be negligible in the ASL context considering the small fraction (approximately 16% (32)) of unextracted water. Moreover, because of longitudinal relaxation, the signal fraction of the initial labelled water ($= e^{-\frac{MTT}{T1b}}$) is only about 4%, assuming an intravascular MTT of 5 s in human brain, and a T_{1b} of 1.66 s. These two mechanisms combine into an amount of tracer signal leakage which is less than 1%. The accuracy of TTT and CTT in absolute terms might also be reduced by CSF contamination in the T1 measurements and by the fact that the relaxation times of labelled water vary between different

compartments, particularly T2, which differs significantly between the intra- and the extravascular space.

In summary, ASL-based transit-time parameters may provide additional diagnostic information, not revealed by CBF measurements alone. For example, the time for intravascular water to distribute from the capillary bed to brain tissue can be related to the capillary function but also to the integrity of the blood brain barrier (BBB). Such additional information might be of relevance in diseases or conditions characterized by disrupted BBB (36,37). Estimates of transfer times reported in this study are in the same range as values of similar or corresponding parameters from previous reports. Although the method does not provide absolute values of physiological parameters, it might still contribute to a more complete picture of the hemodynamic state in brain injury or brain disease. The advantage of the proposed method is that no measurements need to be added to a common time-resolved ASL experiment.

Acknowledgements

This study was supported by the Swedish Research Council (grants no. 13514 and 2010-4454) and The Swedish Cancer Society (grant no. CAN 2012/597).

Appendix

Consider the Fokker-Planck equation for pulsed ASL.

$$\frac{\partial c}{\partial t} = -F\frac{\partial c}{\partial V} + P\frac{\partial^2 c}{\partial V^2} - \frac{c}{T_1}, V \in R, t \geq 0 \qquad [A.1]$$

The Fokker-Planck equation [A.1] (Eq. 10 in Ref. (10)), where F is blood flow and P represents pseudo-diffusion, can be solved using a Fourier transform, taking

into account the initial value stating that the concentration of excited spins at every point in volume V is given by $c=c_0(V',0)$ for t=0, where V' is some known function of the volume. This leads to Eq. [A.2] (i.e., Eq. 15 in Ref. (10)):

$$c(V,t) = \frac{\exp\left(-\frac{t}{T_1}\right)}{\sqrt{4\pi\, Pt}} \int_{-\infty}^{\infty} c_0(V',0) \exp\left(-\frac{(V-V'-Ft)^2}{4\, Pt}\right) \mathrm{d}V' \qquad [A.2]$$

By assuming a rectangular initial condition for the labelling pulse, at t=0, the whole concentration is in the inversion slab, i.e., between the coordinates V=0 and V_b, as illustrated in Figure A1. In analogy with Ref. (10), V is to be interpreted as a coordinate denoting the location of a volume in relation to the labeling plane.

$$c(V,0) = c_0(V) = C_0\big(\theta(V) - \theta(V - V_b)\big), \qquad V_b > 0$$

where $\theta(V)$ is a rectangular function defined as $\theta(V) = 1$ for $V \geq 0$ and $\theta(V) = 0$ for $V < 0$). The concentration of excited spins is zero outside the inversion slab at t=0.

$$c(V,0) = 0, \qquad V > V_b$$

By inserting the above boundary conditions, we obtain

$$c(V,t) =$$

$$\frac{\exp\left(-\frac{t}{T_1}\right)}{\sqrt{4\pi\, Pt}} \int_{-\infty}^{\infty} C_0\big(\theta(V') - \theta(V' - V_b)\big) \exp\left(-\frac{(V-V'-Ft)^2}{4\, Pt}\right) \mathrm{d}V' =$$

$$C_0 \frac{\exp\left(-\frac{t}{T_1}\right)}{\sqrt{4\pi\, Pt}} \int_0^{V_b} \exp\left(-\frac{(V-V'-Ft)^2}{4\, Pt}\right) \mathrm{d}V' \qquad [A.3]$$

For simplicity, a variable substitution $V'' = V - V'$, $\mathrm{d}V'' = -\mathrm{d}V'$ is applied to Eq. [A.3], which gives

$$c(V,t) = C_0 \frac{\exp\left(-\frac{t}{T_1}\right)}{\sqrt{4\pi\, Pt}} \int_{V-V_b}^{V} \exp\left(-\left(\frac{V''-Ft}{\sqrt{4\, Pt}}\right)^2\right) \mathrm{d}V'' \qquad [A.4]$$

According to the definition of the error-function (16), we obtain the following expression:

$$\frac{2}{\sqrt{\pi}} \int_{V-V_b}^{V} \exp\left(-\left(\frac{V''-Ft}{\sqrt{4\, Pt}}\right)^2\right) \mathrm{d}V'' = \left[\mathrm{erf}\left(\frac{V''-Ft}{\sqrt{4\, Pt}}\right)\right]_{V''=V-V_b}^{V''=V} \cdot \sqrt{4\, Pt} \qquad [A.5]$$

By inserting Eq. [A.5] into Eq. [A.4] we get

$$c(V,t) = \frac{C_0}{2} exp\left(-\frac{t}{T_1}\right)\left(\mathrm{erf}\left(\frac{V-Ft}{\sqrt{4\, Pt}}\right) - \mathrm{erf}\left(\frac{V-V_b-Ft}{\sqrt{4\, Pt}}\right)\right) \qquad [A.6]$$

In order to express c(V,t) in terms of time parameters, the following definitions and relationships can be applied:

TTT'=TTT+BL, BL=V_b/F, TTT'=V/F and CTT=P/F^2

These relationships lead to the following set of equations:

$$\frac{V^2}{P} = \frac{F^2 TTT'^2}{F^2 CTT} = \frac{TTT'^2}{CTT}$$
$$\frac{V-Ft}{\sqrt{4\, Pt}} = \frac{TTT'}{\sqrt{4 \cdot CTT \cdot t}} - \frac{t}{\sqrt{4 \cdot CTT \cdot t}} = \frac{TTT'-t}{\sqrt{4 \cdot CTT \cdot t}} \qquad [A.7a]$$

$$\frac{V_b^2}{P} = \frac{F^2 BL^2}{F^2 CTT} = \frac{BL^2}{CTT}$$
$$\frac{V_b-Ft}{\sqrt{4\, Pt}} = \frac{BL}{\sqrt{4 \cdot CTT \cdot t}} - \frac{t}{\sqrt{4 \cdot CTT \cdot t}} = \frac{BL-t}{\sqrt{4 \cdot CTT \cdot t}} \qquad [A.7b]$$

By inserting Eqs [A.7a] and [A.7b] into Eq. [A.6], the final solution can be expressed as follows:

$$c(V,t) = \frac{C_0}{2} \cdot e^{-\frac{t}{T_1}} \left(erf\left(\frac{TTT+BL-t}{\sqrt{4 \cdot CTT \cdot t}}\right) - erf\left(\frac{TTT-t}{\sqrt{4 \cdot CTT \cdot t}}\right)\right) \qquad [A.8]$$

Tables

	ATT [ms] Exp.1	ATT [ms] Exp.2	Mean ATT [ms]	t-Test statistics (two-tailed, df=13)	TTT [ms] Exp. 1	TTT [ms] Exp. 2	CTT [ms] Exp.1	CTT [ms] Exp.2	Mean CTT [ms]	t sta (t d
OC	1330±140	1330±160	1330±150	P<0.0001	1590±110	1600±140	260±60	270±60	270±40	P<
IC	1060±160	1020±120	1040±140		1520±150	1450±160	460±130	420±130	440±130	

Table 1. Average transit time parameters (in ms) for all volunteers, with standard deviation, in the occipital cortex (OC) and insular cortex (IC) for the two experiments. Results of the statistical comparison between the two regions are also shown.

	BAT [ms] Exp. 1	BAT [ms] Exp. 2	Mean BAT [ms]	t-Test statistics (two-tailed, df=13)	BL[ms] Exp.1	BL [ms] Exp.2
OC	560±130	540±140	550±120	p<0.0001	1120±60	1110±60
IC	370±100	360±80	370±80		960±120	940±80

Table 2. Average bolus arrival time and bolus length for all volunteers, with standard deviation, in the occipital lobe (OC) and insular cortex (IC) for the two experiments. Results of the statistical comparison between the two regions are also shown.

References

1. Kaufmann AM, Firlik AD, Fukui MB, Wechsler LR, Jungries CA, Yonas H. Ischemic core and penumbra in human stroke. Stroke 1999; 30: 93-99.
2. Berman KF, Torrey EF, Daniel DG, Weinberger DR. Regional cerebral blood flow in monozygotic twins discordant and concordant for schizophrenia. Arch. Gen. Psychiatry 1992; 49: 927-934.
3. Dousse M, Mamo H, Ponsin JC, Tran Dinh Y. Cerebral blood flow in schizophrenia. Exp. Neurol. 1988; 100: 98-111.
4. Wolk DA, Detre JA. Arterial spin labeling MRI: An emerging biomarker for Alzheimer's disease and other neurodegenerative conditions. Curr. Opin. Neurol. 2012; 25: 421-428.
5. Gregori J, Schuff N, Kern R, Gunther M. T2-based arterial spin labeling measurements of blood to tissue water transfer in human brain. J. Magn. Reson. Imaging 2013; 37: 332-342.
6. Wells JA, Siow B, Lythgoe MF, Thomas DL. Measuring biexponential transverse relaxation of the ASL signal at 9.4 T to estimate arterial oxygen saturation and the time of exchange of labeled blood water into cortical brain tissue. J. Cereb. Blood Flow Metab. 2013; 33: 215-224.
7. Stanisz GJ, Odrobina EE, Pun J, Escaravage M, Graham SJ, Bronskill MJ, Henkelman RM. T1, T2 relaxation and magnetization transfer in tissue at 3T. Magn. Reson. Med. 2005; 54: 507-512.
8. Wells JA, Lythgoe MF, Choy M, Gadian DG, Ordidge RJ, Thomas DL. Characterizing the origin of the arterial spin labelling signal in MRI using a multiecho acquisition approach. J. Cereb. Blood Flow Metab. 2009; 29: 1836-1845.
9. Wang J, Fernandez-Seara MA, Wang S, St Lawrence KS. When perfusion meets diffusion: In vivo measurement of water permeability in human brain. J. Cereb. Blood Flow Metab. 2007; 27: 839-849.
10. Kelly ME, Blau CW, Kerskens CM. Bolus-tracking arterial spin labelling: Theoretical and experimental results. Phys. Med. Biol. 2009; 54: 1235-1251.
11. Alsop DC, Detre JA. Reduced transit-time sensitivity in noninvasive magnetic resonance imaging of human cerebral blood flow. J. Cereb. Blood Flow Metab. 1996; 16: 1236-1249.
12. Gunther M, Oshio K, Feinberg DA. Single-shot 3D imaging techniques improve arterial spin labeling perfusion measurements. Magn. Reson. Med. 2005; 54: 491-498.
13. Bibic A, Knutsson L, Ståhlberg F, Wirestam R. Denoising of arterial spin labeling data: Wavelet-domain filtering compared with gaussian smoothing. Magn. Reson. Mater. Phy. 2010; 23: 125-137.
14. Siversson C, Tiderius CJ, Dahlberg L, Svensson J. Local flip angle correction for improved volume T1-quantification in three-dimensional dGEMRIC using the Look-Locker technique. J. Magn. Reson. Imaging 2009; 30: 834-841.
15. Buxton RB, Frank LR, Wong EC, Siewert B, Warach S, Edelman RR. A general kinetic model for quantitative perfusion imaging with arterial spin labeling. Magn. Reson. Med. 1998; 40: 383-396.
16. Cody WJ. Rational Chebyshev approximations for the error function. Mathematics of Computation 1969; 23: 631-637.
17. Lu H, Clingman C, Golay X, van Zijl PC. Determining the longitudinal relaxation time (T1) of blood at 3.0 tesla. Magn. Reson. Med. 2004; 52: 679-682.
18. James F, Roos M. Minuit – a system for function minimization and analysis of the parameter errors and correlations. Computer Physics Communications 1975; 10: 343-367.

19. Zhou JY, Wilson DA, Ulatowski JA, Trajstman RJ, van Zijl PCM. Two-compartment exchange model for perfusion quantification using arterial spin tagging. J. Cereb. Blood Flow Metab. 2001; 21: 440-455.
20. Levick JR, Michel CC. Microvascular fluid exchange and the revised starling principle. Cardiovasc. Res. 2010 ;87: 198-210.
21. Wink AM, Roerdink JB. Denoising functional MR images: A comparison of wavelet denoising and gaussian smoothing. IEEE Trans. Med. Imaging 2004; 23: 374-387.
22. Kim SG. Quantification of relative cerebral blood flow change by flow-sensitive alternating inversion recovery (FAIR) technique: Application to functional mapping. Magn. Reson. Med. 1995; 34: 293-301.
23. Wong EC, Buxton RB, Frank LR. Quantitative imaging of perfusion using a single subtraction (QUIPSS and QUIPSS II). Magn. Reson. Med. 1998; 39: 702-708.
24. Luh WM, Wong EC, Bandettini PA, Hyde JS. QUIPSS II with thin-slice TI1 periodic saturation: A method for improving accuracy of quantitative perfusion imaging using pulsed arterial spin labeling. Magn. Reson. Med. 1999; 41: 1246-1254.
25. Parkes LM, Tofts PS. Improved accuracy of human cerebral blood perfusion measurements using arterial spin labeling: Accounting for capillary water permeability. Magn. Reson. Med. 2002; 48: 27-41.
26. St Lawrence KS, Frank JA, McLaughlin AC. Effect of restricted water exchange on cerebral blood flow values calculated with arterial spin tagging: A theoretical investigation. Magn. Reson. Med. 2000; 44: 440-449.
27. Wu WC, Mazaheri Y, Wong EC. The effects of flow dispersion and cardiac pulsation in arterial spin labeling. IEEE Trans. Med. Imaging 2007; 26: 84-92.
28. Kazan SM, Chappell MA, Payne SJ. Modeling the effects of flow dispersion in arterial spin labeling. IEEE Trans. Biomed. Eng. 2009; 56: 1635-1643.
29. Cavusoglu M, Pohmann R, Burger HC, Uludag K. Regional effects of magnetization dispersion on quantitative perfusion imaging for pulsed and continuous arterial spin labeling. Magn. Reson. Med. 2013; 69: 524-530.
30. Paulson OB, Hertz MM, Bolwig TG, Lassen NA. Filtration and diffusion of water across blood-brain-barrier in man. Microvascular Research 1977; 13: 113-123.
31. Berridge MS, Adler LP, Nelson AD, Cassidy EH, Muzic RF, Bednarczyk EM, Miraldi F. Measurement of human cerebral blood-flow with [O-15]butanol and positron emission tomography. J. Cereb. Blood Flow Metab. 1991; 11: 707-715.
32. Herscovitch P, Raichle ME, Kilbourn MR, Welch MJ. Positron emission tomographic measurement of cerebral blood flow and permeability-surface area product of water using [15O]water and [11C]butanol. J. Cereb. Blood Flow Metab. 1987; 7: 527-542.
33. Wong EC, Buxton RB, Frank LR. Implementation of quantitative perfusion imaging techniques for functional brain mapping using pulsed arterial spin labeling. NMR Biomed. 1997; 10: 237-249.
34. Leenders KL, Perani D, Lammertsma AA, Heather JD, Buckingham P, Healy MJ, Gibbs JM, Wise RJ, Hatazawa J, Herold S, Beaney RP, Brooks DJ, Spinks T, Rhodes C, Frackowiak RS, Jones T. Cerebral blood flow, blood volume and oxygen utilization. Normal values and effect of age. Brain 1990; 113: 27-47.
35. Ito H, Kanno I, Iida H, Hatazawa J, Shimosegawa E, Tamura H, Okudera T. Arterial fraction of cerebral blood volume in humans measured by positron emission tomography. Ann. Nucl. Med. 2001; 15: 111-116.
36. Ballabh P, Braun A, Nedergaard M. The blood-brain barrier: An overview: Structure, regulation, and clinical implications. Neurobiol. Dis. 2004; 16: 1-13.
37. Bradbury MW. The blood-brain barrier. Exp. Physiol. 1993; 78: 453-472.

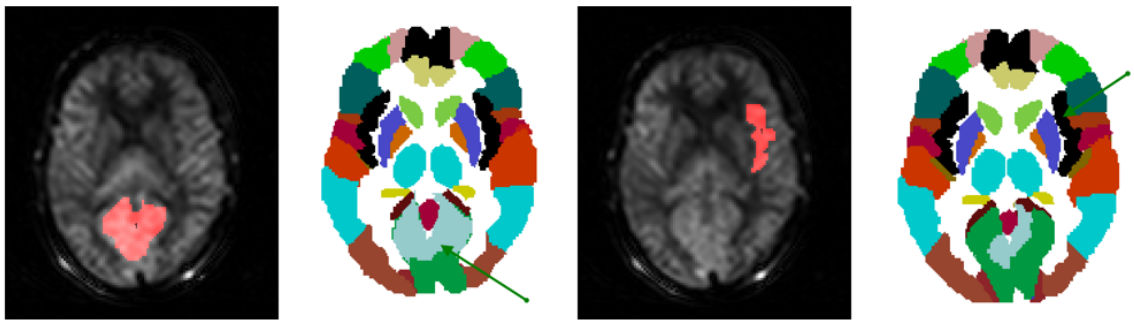

Figure 1. ROIs overlaid on the ASL-weighted maps. The occipital lobe (OC), i.e., a mixture of calcarine sulcus [visual cortex], precuneus and cignuli posterior (left) and the corresponding AAL map (middle-left). Insular cortex (IC) (middle-right) and the corresponding AAL map (right).

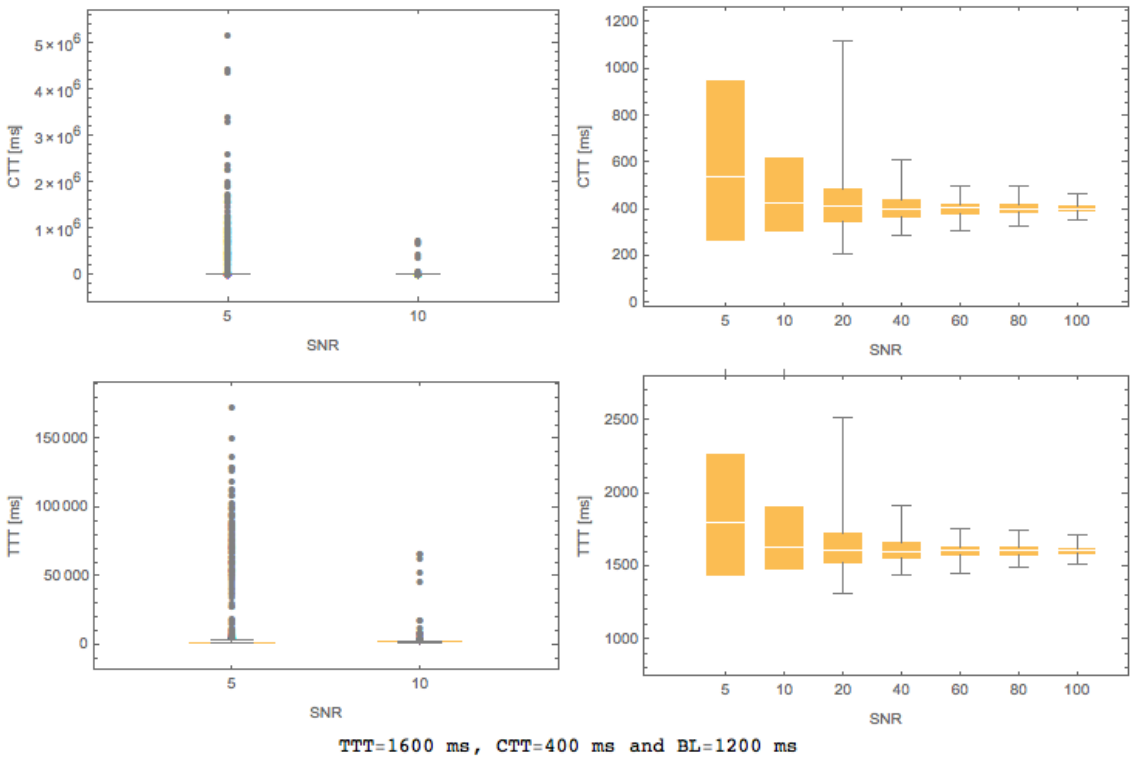

Figure 2. Box-and-whiskers plots of CTT (top row) and TTT (bottom row) data distributions for input values of TTT=1600 ms, CTT=400 ms and BL=1200 ms, and for different SNR values used in the simulations. The top and bottom edges of the box represent the upper and lower quartiles (the interquartile range or IQR), respectively, the whiskers represent the minimum value on one side and the values up to 1.5xIQR from the quartile on the other side, with dots on this end of the plot representing outliers.

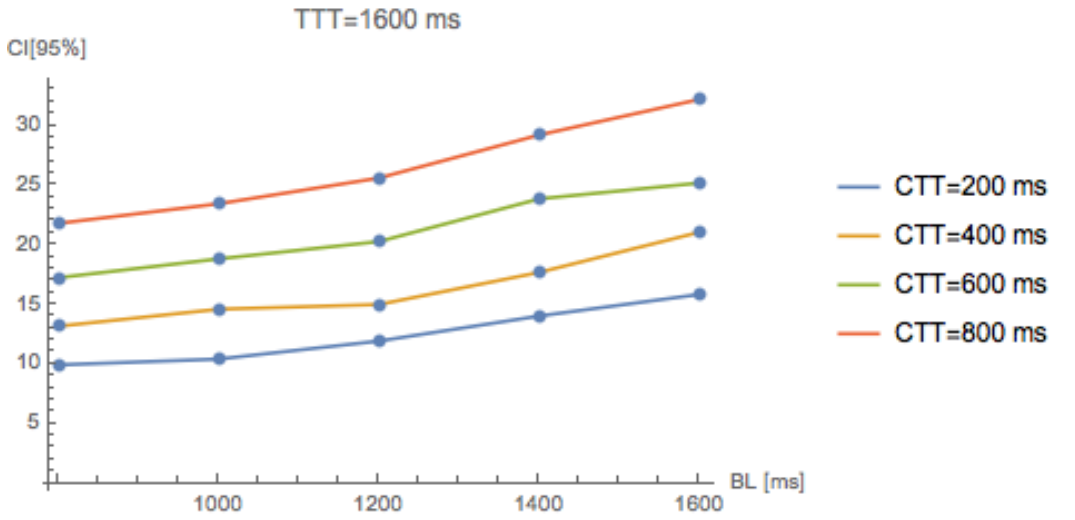

Figure 3. The simulated 95% confidence interval in percent of the true value of CTT (for different CTTs) as a function of BL, for TTT=1600 ms.

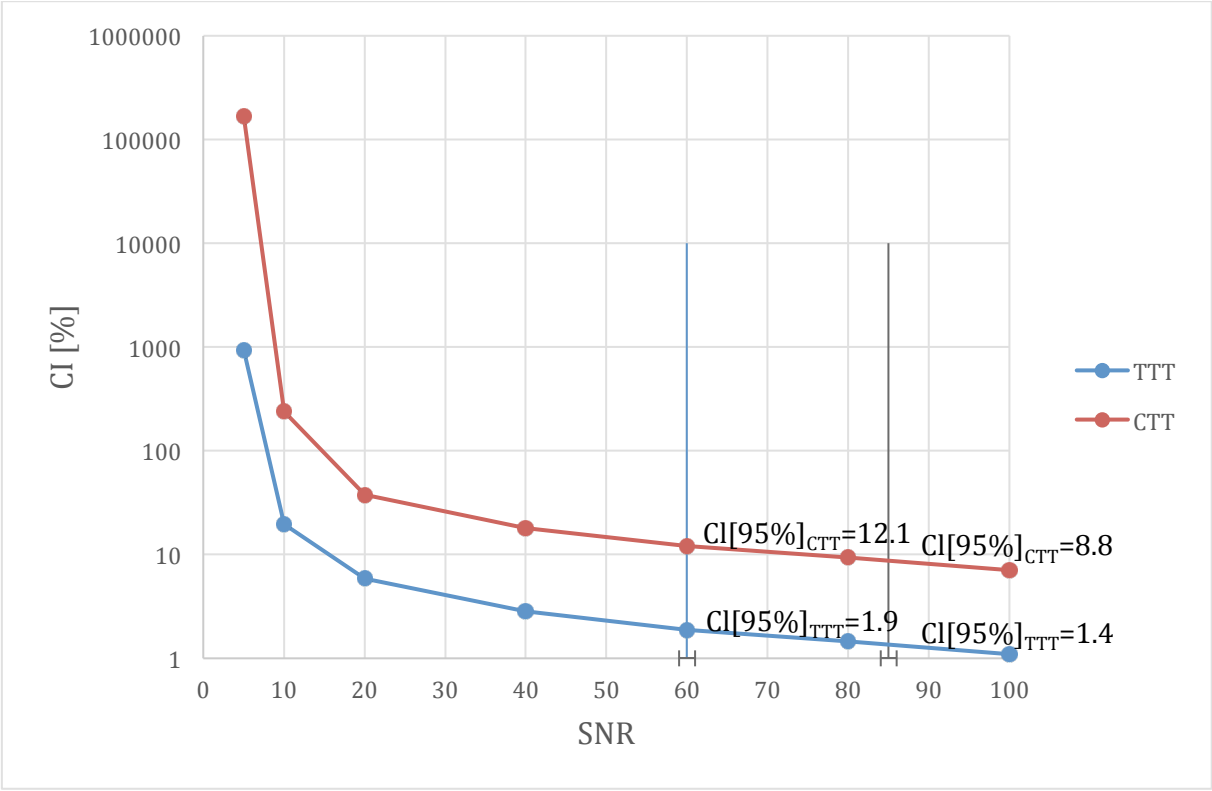

Figure 4. Width of the confidence interval in percent of the true values of TTT (blue line) and CTT (red line) as a function of SNR for TTT=1600 ms, CTT=200 ms and BL=1200 ms, used in the simulations. SNR levels corresponding to the two experimental ROIs are indicated by vertical lines.

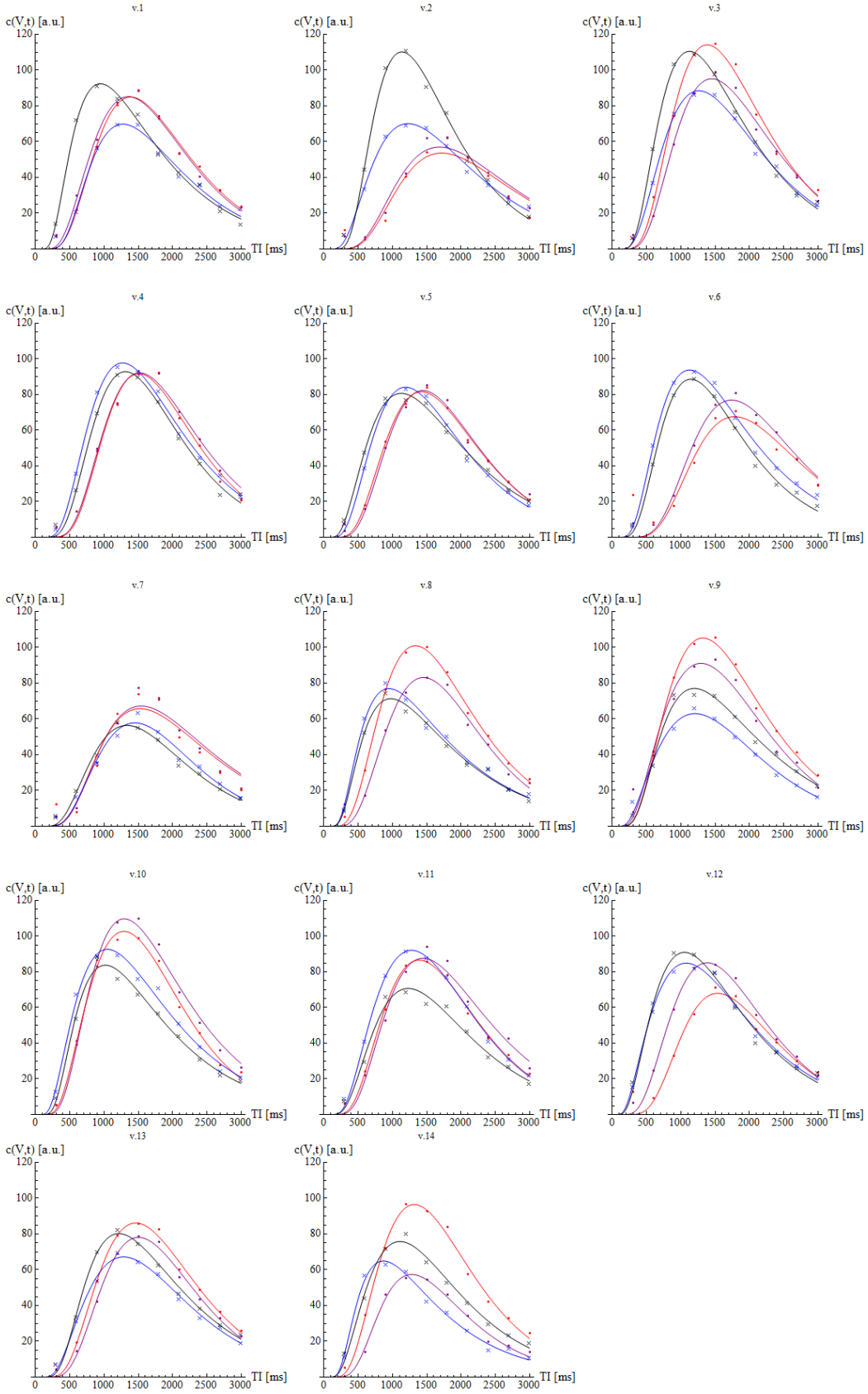

Figure 5. Dynamic ASL signal time courses for all 14 volunteers. Data points corresponding to the occipital lobe are indicated by purple dots (first experiment) and red dots (second experiment). Data corresponding to the insular cortex are indicated by

blue crosses (first experiment) and black crosses (second experiment). Model fits are shown as solid lines in the corresponding colors.

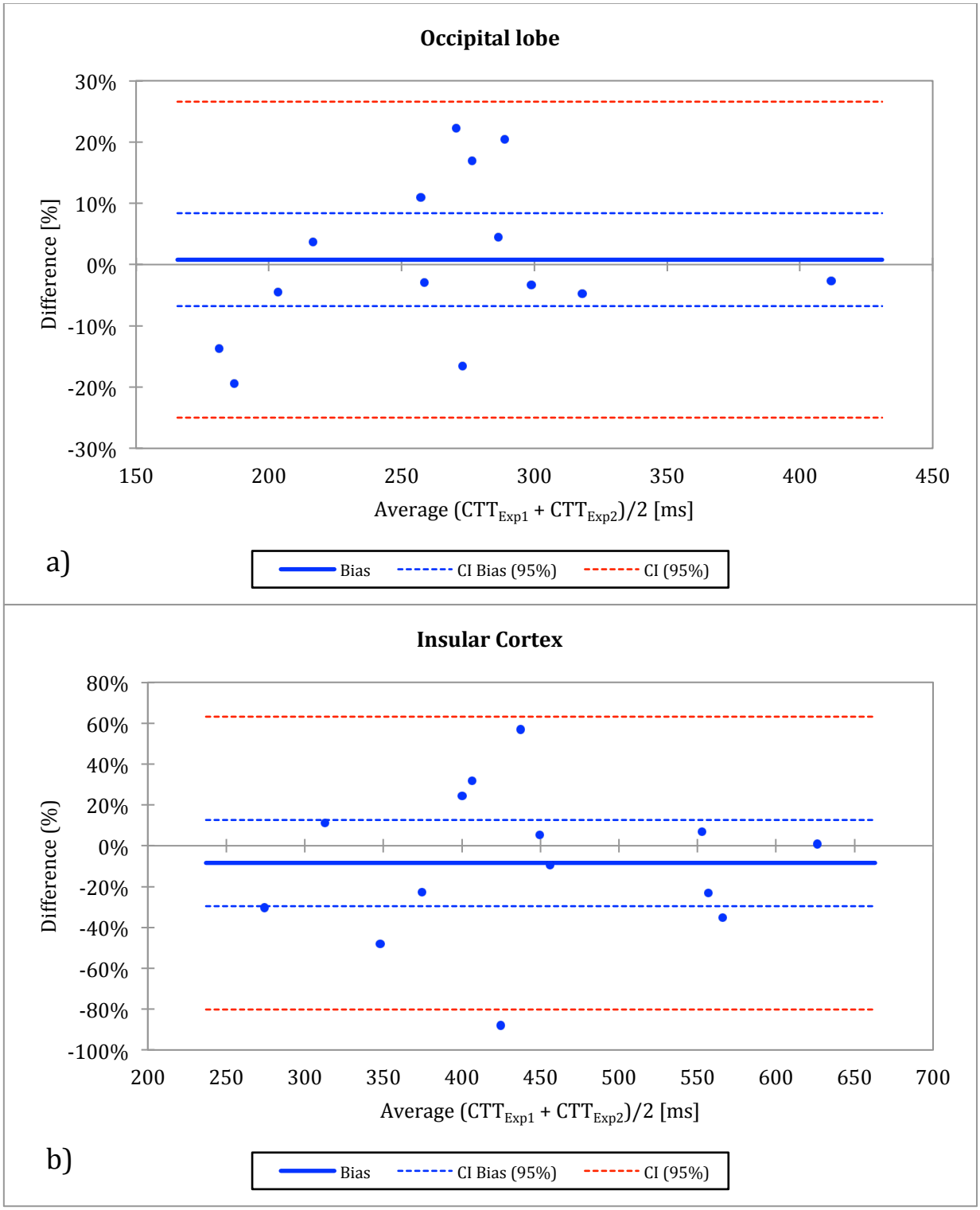

Figure 6. Bland-Altman plots, i.e., relative differences between the CTT values from the two experiments plotted against the test-retest mean value in a) the occipital lobe (OC) and b) the insular cortex (IC). The solid horizontal blue line is the mean difference (less than 4% and 9% in OC

and IC, respectively), red dashed lines are defined as the mean difference ±1.96 times the standard deviation of the differences and the blue dashed lines are 95% CI of the mean of differences.

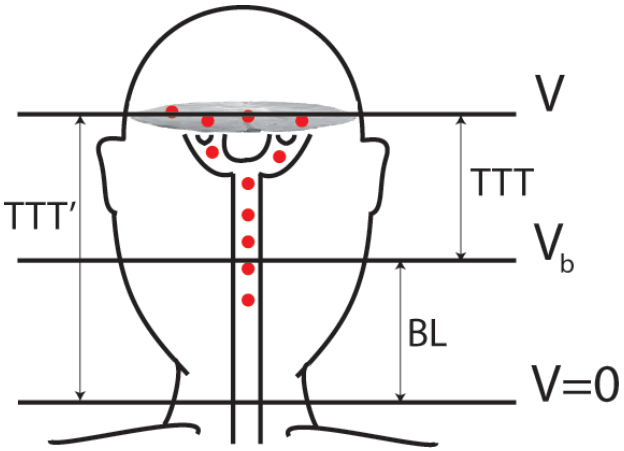

Figure A 1: Schematic graphic representation of the current model. Coordinates V_b and V=0 represent the front and rear edges of the inversion slab, respectively, V denotes the location where the measurement in tissue occurs. BL is the bolus length, and TTT and TTT' are the total transit times from V_b and V=0, respectively, to location V.

Tables

	ATT [ms] Exp.1	ATT [ms] Exp.2	Mean ATT [ms]	t-Test statistics (two-tailed, df=13)	TTT [ms] Exp. 1	TTT [ms] Exp. 2	CTT [ms] Exp.1	CTT [ms] Exp.2	Mean CTT [ms]	t-Te statis (two taile df=1
OC	1330±140	1330±160	1330±150	P<0.0001	1590±110	1600±140	260±60	270±60	270±40	P<0.0
IC	1060±160	1020±120	1040±140		1520±150	1450±160	460±130	420±130	440±130	

Table 1. Average transit time parameters (in ms) for all volunteers, with standard deviation, in the occipital cortex (OC) and insular cortex (IC) for the two experiments. Results of the statistical comparison between the two regions are also shown.

	BAT [ms] Exp. 1	BAT [ms] Exp. 2	Mean BAT [ms]	t-Test statistics (two-tailed, df=13)	BL[ms] Exp.1	BL [ms] Exp.2
OC	560±130	540±140	550±120	p<0.0001	1120±60	1110±60
IC	370±100	360±80	370±80		960±120	940±80

Table 2. Average bolus arrival time and bolus length for all volunteers, with standard deviation, in the occipital lobe (OC) and insular cortex (IC) for the two experiments. Results of the statistical comparison between the two regions are also shown.

Supplementary material

Supplementary figures

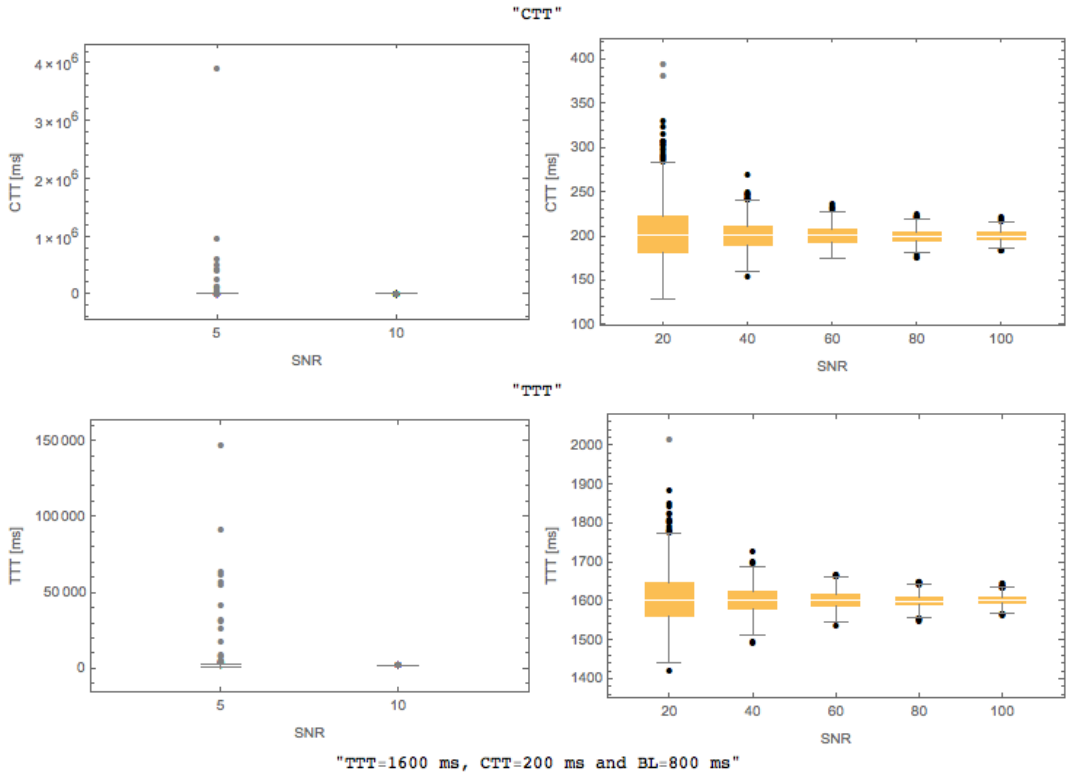

Figure S1a: Box-and-whiskers plots of CTT (top row) and TTT (bottom row) data distributions for input values of TTT=1600 ms, CTT=200 ms and BL=800 ms and for different SNR values used in the simulations. The top and bottom edges of the box represent the upper and lower quartiles (the interquartile range or IQR), respectively, the whiskers represent the minimum value on one side and the values up to 1.5xIQR from the quartile on the other side, with dots on this end of the plot representing outliers.

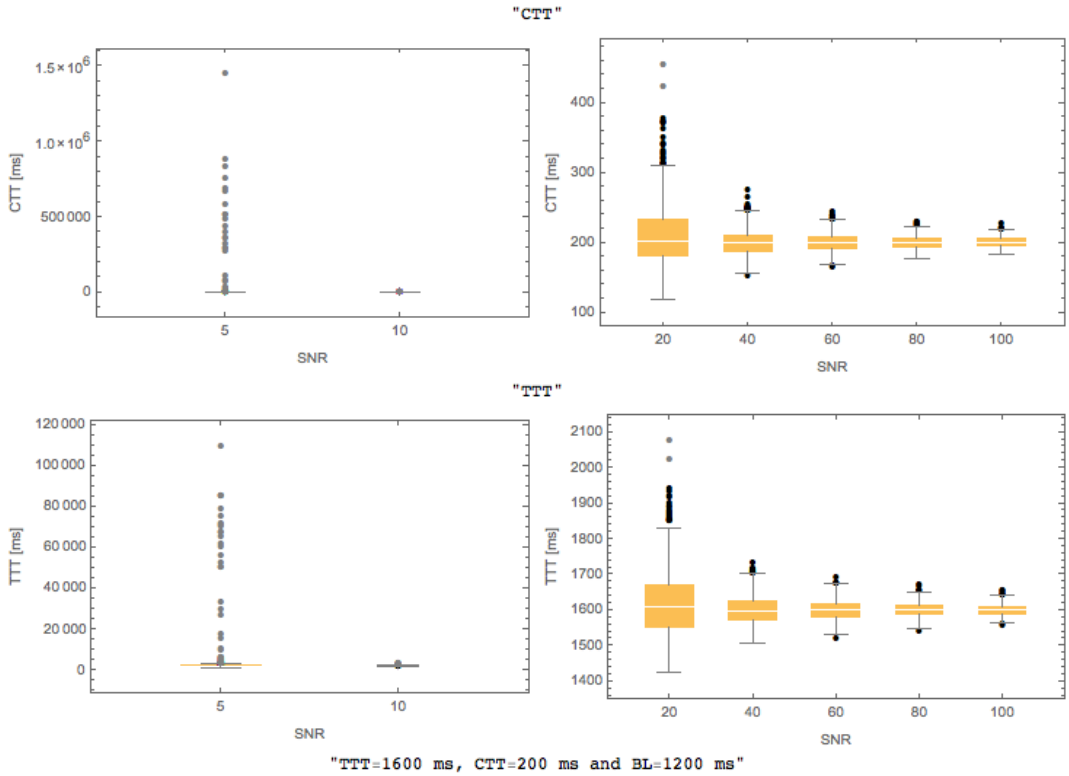

Figure S1b: Box-and-whiskers plots of CTT (top row) and TTT (bottom row) data distributions for input values of TTT=1600 ms, CTT=200 ms and BL=1200 ms and for different SNR values used in the simulations. The top and bottom edges of the box represent the upper and lower quartiles (the interquartile range or IQR), respectively, the whiskers represent the minimum value on one side and the values up to 1.5xIQR from the quartile on the other side, with dots on this end of the plot representing outliers.

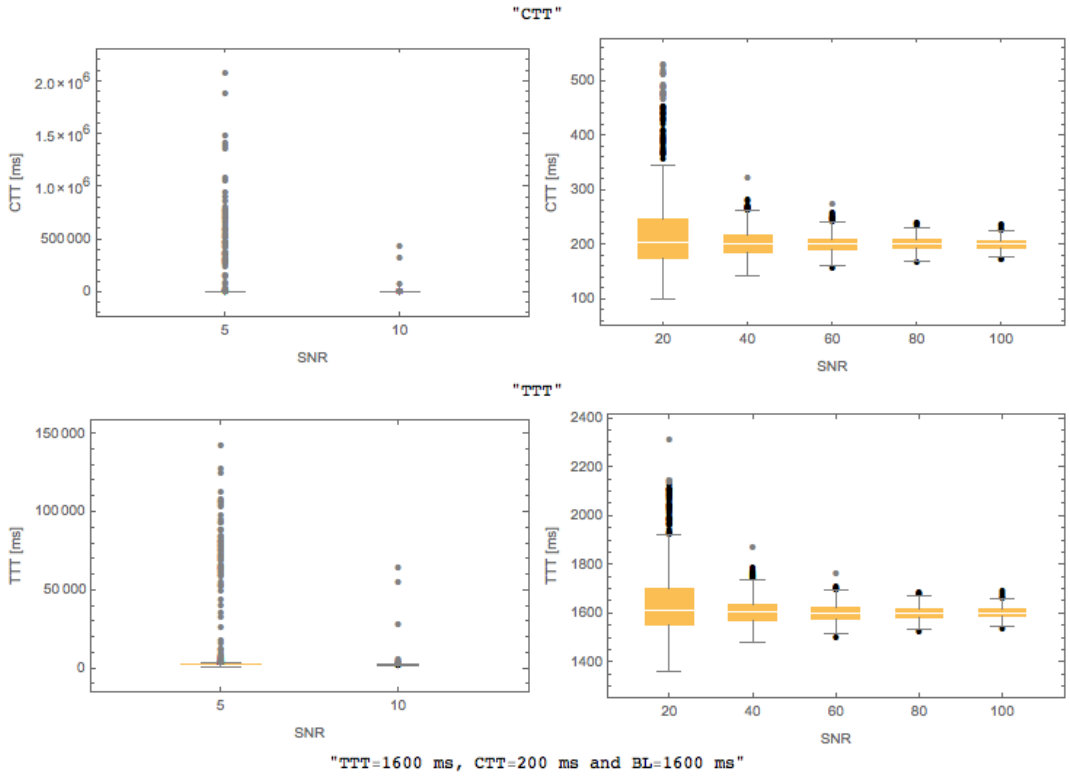

Figure S1c: Box-and-whiskers plots of CTT (top row) and TTT (bottom row) data distributions for input values of TTT=1600 ms, CTT=200 ms and BL=1600 ms and for different SNR values used in the simulations. The top and bottom edges of the box represent the upper and lower quartiles (the interquartile range or IQR), respectively, the whiskers represent the minimum value on one side and the values up to 1.5xIQR from the quartile on the other side, with dots on this end of the plot representing outliers.

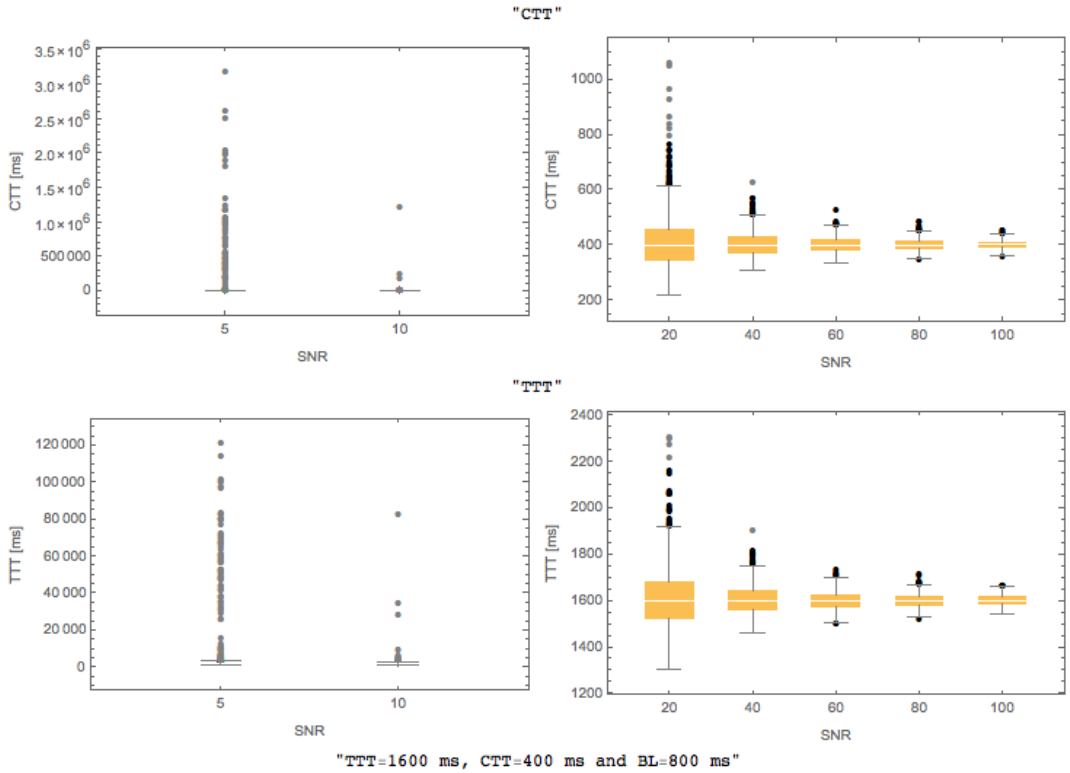

Figure S2a: Box-and-whiskers plots of CTT (top row) and TTT (bottom row) data distributions for input values of TTT=1600 ms, CTT=400 ms and BL=800 ms and for different SNR values used in the simulations. The top and bottom edges of the box represent the upper and lower quartiles (the interquartile range or IQR), respectively, the whiskers represent the minimum value on one side and the values up to 1.5xIQR from the quartile on the other side, with dots on this end of the plot representing outliers.

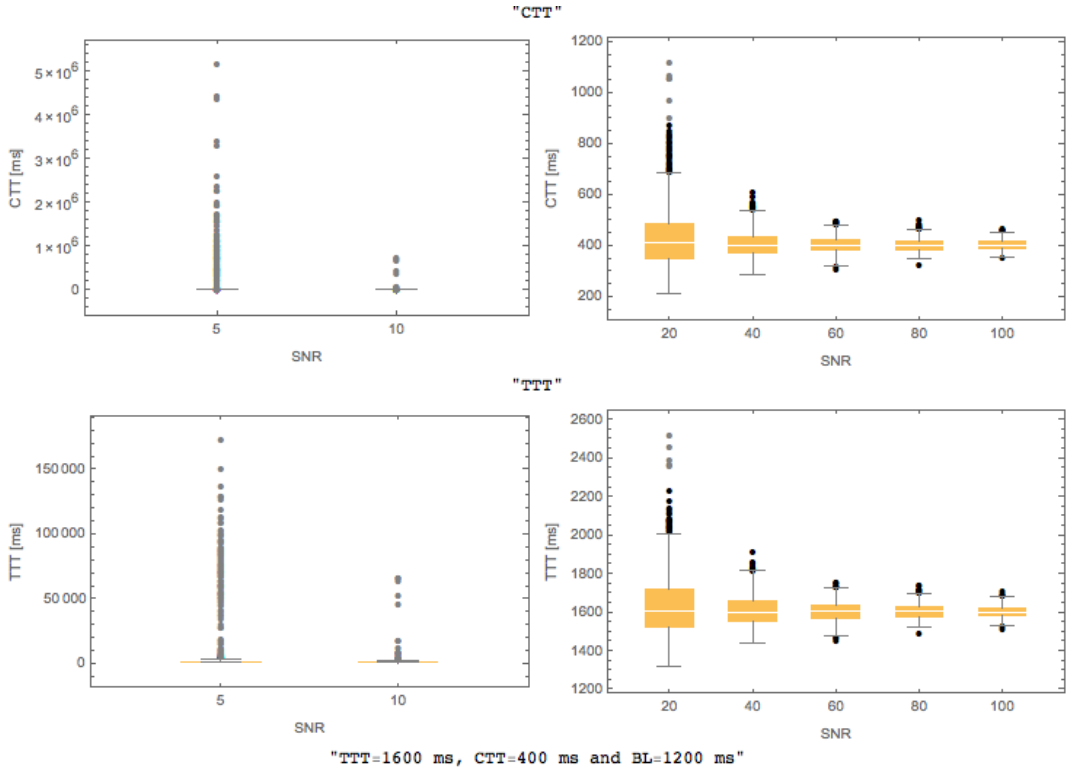

Figure S2b: Box-and-whiskers plots of CTT (top row) and TTT (bottom row) data distributions for input values of TTT=1600 ms, CTT=400 ms and BL=1200 ms and for different SNR values used in the simulations. The top and bottom edges of the box represent the upper and lower quartiles (the interquartile range or IQR), respectively, the whiskers represent the minimum value on one side and the values up to 1.5xIQR from the quartile on the other side, with dots on this end of the plot representing outliers.

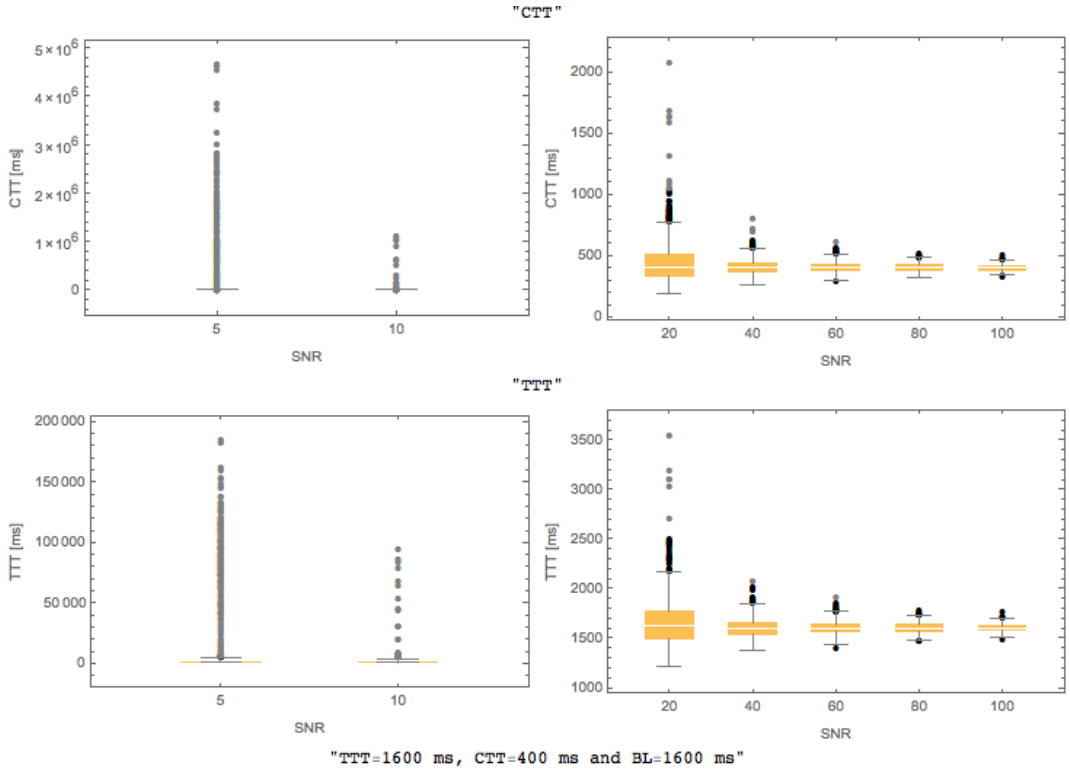

Figure S2c: Box-and-whiskers plots of CTT (top row) and TTT (bottom row) data distributions for input values of TTT=1600 ms, CTT=400 ms and BL=1600 ms and for different SNR values used in the simulations. The top and bottom edges of the box represent the upper and lower quartiles (the interquartile range or IQR), respectively, the whiskers represent the minimum value on one side and the values up to 1.5xIQR from the quartile on the other side, with dots on this end of the plot representing outliers.

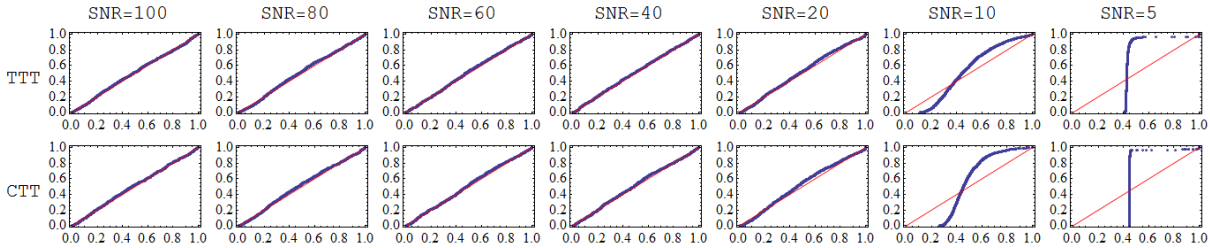

Figure S3: So-called probability-probability plots (P-P plots) for the simulated distributions of TTT and CTT estimates (true values TTT=1600 ms and CTT=200 ms) at different SNR levels and BL=1200 ms. The simulated cumulative distribution functions (CDFs) (y-axis) are plotted against the theoretical CDF of a normal distribution (x-axis). The red line represents the CDFs of two normal distributions plotted against each other. The P-P plot introduces a goodness of fit test based on the correlation between sample and theoretical probabilities. The distributions are equal if and only if the plot falls on the unity line (red line), and any deviation indicates a difference between the distributions. ("Testing for Normality" by Henry C. Thode, CRC Press, 2002, ISBN 978-0-8247-9613-6)

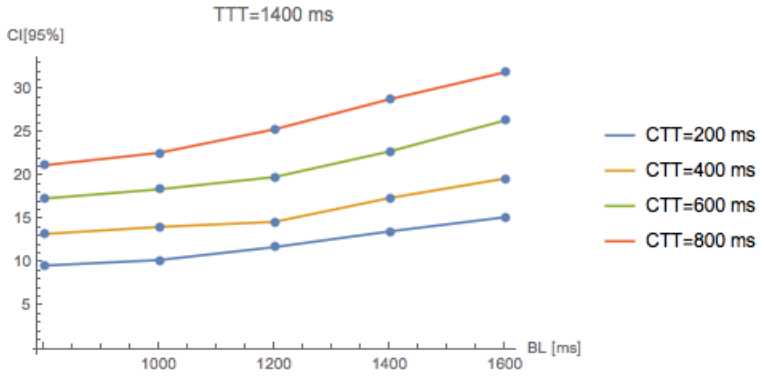

Figure S4a: The simulated 95% confidence interval in percent of the true value of CTTs (for different CTTs) as a function of BL, for TTT=1400 ms.

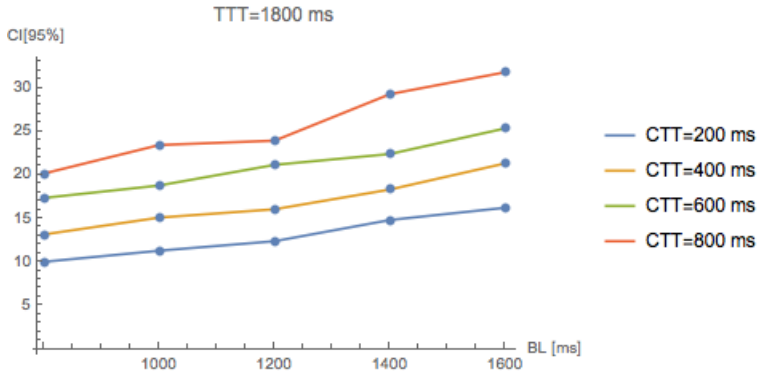

Figure S4b: The simulated 95% confidence interval in percent of the true value of CTTs (for different CTTs) as a function of BL, for TTT=1800 ms.

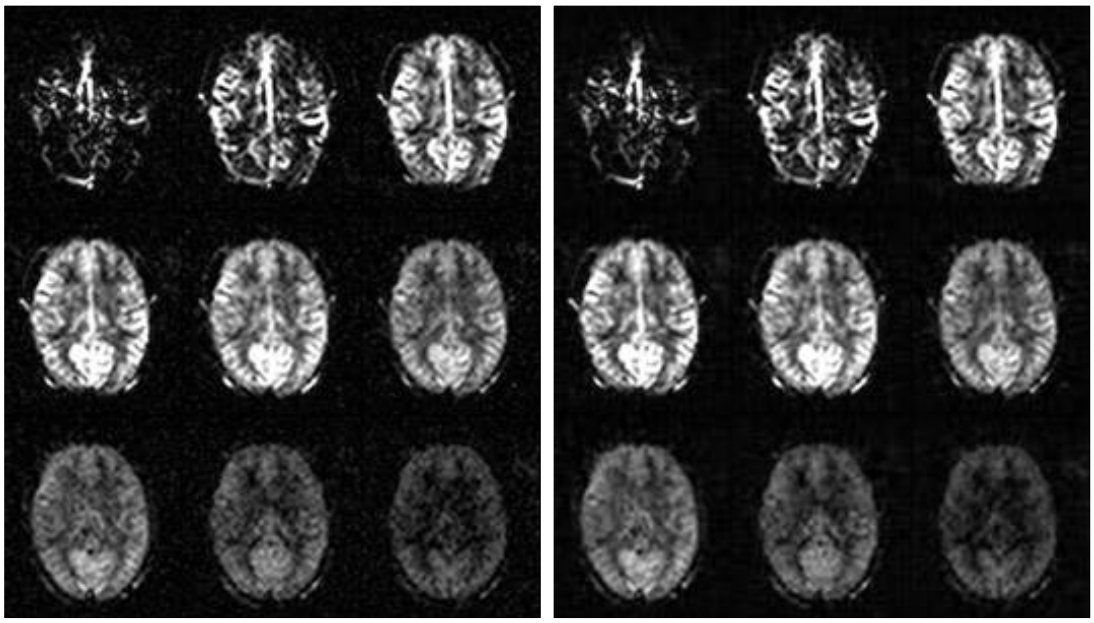

Figure S5. Examples of ASL difference maps for varying inversion time TI, ranging from 600 to 3000 ms at intervals of 300 ms. Images before (left panel) and after (right panel) the denoising procedure.